ISSN 0021-8944, Journal of Applied Mechanics and Technical Physics, 2017, Vol. 58, No. 3, pp. 386–391. © Pleiades Publishing, Ltd., 2017.
Original Russian Text © S. Gholampour, N. Fatouraee, A.S. Seddighi, A. Seddighi.

NUMERICAL SIMULATION OF CEREBROSPINAL FLUID HYDRODYNAMICS IN THE HEALING PROCESS OF HYDROCEPHALUS PATIENTS

S. Gholampour[a], N. Fatouraee[b], A. S. Seddighi[c], and A. Seddighi[c]

UDC 612.8; 532.5

Abstract: Three-dimensional computational models of the cerebrospinal fluid (CSF) flow and brain tissue are presented for evaluation of their hydrodynamic conditions before and after shunting for seven patients with non-communicating hydrocephalus. One healthy subject is also modeled to compare deviated patients data to normal conditions. The fluid-solid interaction simulation shows the CSF mean pressure and pressure amplitude (the superior index for evaluation of non-communicating hydrocephalus) in patients at a greater point than those in the healthy subject by 5.3 and 2 times, respectively.

Keywords: aqueduct of sylvius, CSF pressure, fluid-solid interactions, Reynolds number, shunting.

DOI: 10.1134/S0021894417030026

INTRODUCTION

The cerebrospinal fluid (CSF) is produced in the choroid plexus of the lateral ventricles and flows toward the third ventricle, through the aqueduct of Sylvius (AS), to the fourth ventricle and the subarachnoid space. The cause of non-communicating hydrocephalus (NCH) in most cases is the obstruction or blockage of the CSF flow pathway [1]. Cerebral shunting is a common treatment for NCH [1]. There are two groups of studies in the scientific literature which are related to this research: clinical research and computer modeling. Malm et al. [2] and Eide and Brean [3] compared the clinical CSF pressure data determined before and after shunting. They used the intracranial pressure (ICP) (not the intraventricular pressure (IVP)) as the index for disease evaluation. Many researches of this group (clinical methods) used invasive techniques to measure the CSF pressure. However, it is not possible to take accurate undistorted measurements while using a clinical method without surgery [4]. Additionally, the inherent complexity of the CSF flow makes clinical methods not suitable for the CSF flow analysis [4]. Therefore, computer modeling becomes an important method for studying NCH. Other groups of researchers calculated the CSF biofluid parameters of hydrocephalus patients by using 3D computer modeling [4–6]. The effect of shunt treatment and the manner of changes in the CSF hydrodynamic indices during the treatment process, however, have not yet been simulated.

The effects of CSF hydrodynamic parameter changes in NCH patients are investigated in this work by a non-invasive method, and the changes in the CSF pressure in the AS (between the third and fourth ventricles) before and after shunting in a two-year follow-up period are analyzed.

[a]Department of Biomedical Engineering, Science and Research Branch, Islamic Azad University, Tehran, Iran. [b]Biological Fluid Mechanics Research Laboratory, Biomechanics Department, Biomedical Engineering Faculty, Amirkabir University of Technology, [c]Functional Neurosurgery Research Center of Shohada Tajrish Hospital, Shahid Beheshti University of Medical Sciences, Tehran, Iran; s.gholampour@srbiau.ac.ir, nasser@aut.ac.ir, a_sedighi@sbmu.ac.ir, afsounseddighi@sbmu.ac.ir. Translated from Prikladnaya Mekhanika i Tekhnicheskaya Fizika, Vol. 58, No. 3, pp. 12–18, May–June, 2017. Original article submitted February 20, 2016.

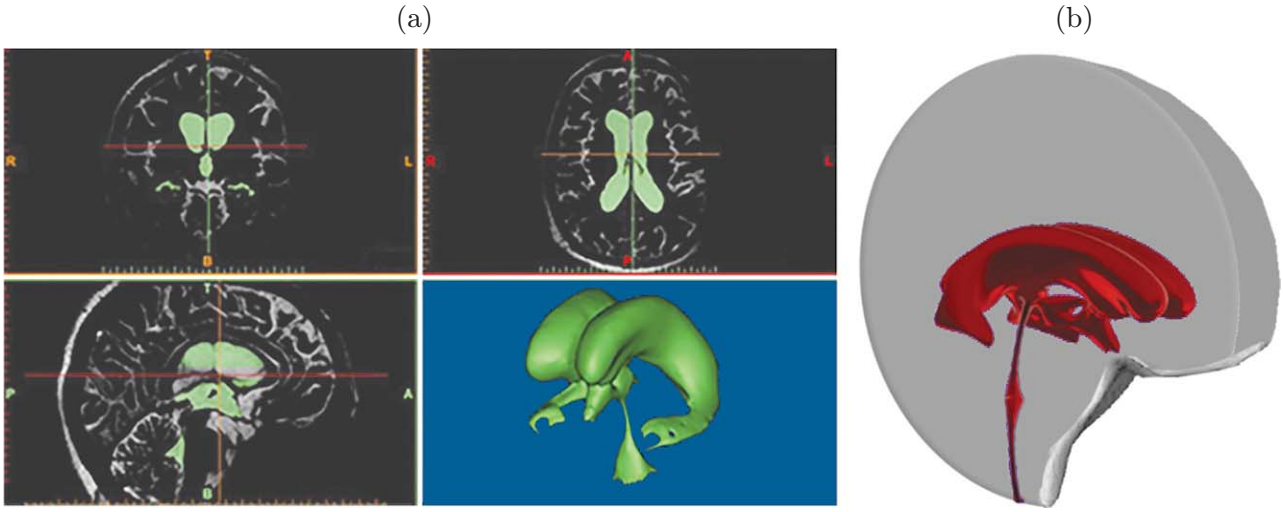

Fig. 1. Results of scanning and 3D model: (a) point cloud of the ventricular system; (b) 3D model of the ventricular system and brain tissue.

1. MATERIAL AND METHODS

The model and methods used in studying the CSF flow are described below.

1.1. Model

Seven NCH patients with stenosis in the AS were selected for this study. One healthy subject was used to compare deviated data from normal conditions. The average (for seven patients) height, weight, and age of patients were (1.60 ± 0.12) m, (68.2 ± 8.8) kg, and (31.6 ± 9.6) years, respectively. These parameters were 1.6 m, 68.2 kg, and 27 years for the healthy subject. Cine phase-contrast magnetic resonance imaging (CINE PC-MRI) acquisition procedures were undertaken for each of the seven patients and the healthy subject's heads. All scans were performed with a 3T MRI unit for both the patients and the healthy subject in the supine position during the examinations. Algin et al. [7] provided more detailed information about this imaging protocol and scan conditions.

The first obtained output of CINE PC-MRI was a set of DICOM files of the heads of each of the patients and the healthy subject. The extracted point cloud (obtained from DICOM files) (Fig. 1a) was utilized to build 3D models (Fig. 1b) of the ventricular system and brain tissue, which were then used for meshing and numerical analysis. The second obtained output of CINE PC-MRI was a set of temporal velocity diagrams of the CSF in the AS of each of the patients and the healthy subject, which were used to compare numerical simulated data with experimental data. Patients were treated by using cerebral ventriculoperitoneal shunts (VPS) with differential pressure valves (Cordis Hakim standard system), based on the diagnosis and advice of the specialist physician.

1.2. Fluid-Solid Interaction Method

We use a fluid-solid interaction (FSI) method for simultaneous analysis of the CSF flow and brain tissue. The brain tissue was considered as a solid domain, while the ventricular system was considered as a fluid domain; therefore, the interface between the CSF and brain tissue was considered as a deformable boundary. However, some studies did not consider this interaction, and the analysis was performed with considering the CSF and brain tissue independently. Other studies used alternative methods, such as computational fluid dynamics (CFD) simulations [4, 5].

Regarding the use of the FSI approach and the Arbitrary Lagrangian — Eulerian (ALE) equations for simultaneous analysis of the equations governing the solid and fluid domains, the governing equations are as follows. The solid domain is formulated by using the Lagrangian model

$$\frac{\partial \tau_{ij}^{s}}{\partial x_j} = \rho^{s} \frac{\partial^2 d_i^{s}}{\partial t^2},$$

where ρ^s, d_i^s, and τ_{ij}^s are the density, boundary displacement, and Cauchy stress tensor in the brain tissue, respectively.

The CSF flow is defined as an isothermal incompressible Newtonian fluid [8]:

$$\frac{1}{\beta}\frac{\partial p}{\partial t} + \frac{\partial u_i}{\partial x_i} = 0, \qquad \rho^f \frac{\partial u_i}{\partial t} + \rho^f \Big(u_j - \frac{\partial d_j^f}{\partial t}\Big)\frac{\partial u_i}{\partial x_j} = \frac{\partial \tau_{ij}^f}{\partial x_j}.$$

Here β is the bulk coefficient, p is the pressure, u_i are the velocity vector components, ρ^f is the fluid density, d_j^f are the components of the fluid domain displacements, and τ_{ij}^f is the Cauchy stress tensor defined as

$$\tau_{ij}^f = -p\delta_{ij} + 2\mu e_{ij}, \qquad e_{ij} = \frac{1}{2}\Big(\frac{\partial u_i}{\partial x_j} + \frac{\partial u_j}{\partial x_i}\Big),$$

where δ_{ij} is the Kronecker delta, μ is the CSF viscosity, and e_{ij} are the strain tensor components.

1.3. CSF and Brain Tissue Properties

In this study, the CSF is treated as a Newtonian fluid with a dynamic viscosity and density equal to $1.003 \cdot 10^{-3}$ kg/(m · s) and 998.2 kg/m^3, respectively [5]. The brain tissue is considered as a linear viscoelastic material with the storage and loss moduli of 2038 and 1356 Pa for the healthy subject and 1594 and 1015 Pa for the patients, and the density of 1040 kg/m^3 [8, 9]. The CSF flow rate in the lateral ventricles is 0.35 cm^3/min [1] This value is used as the amplitude in the input fluid pulsatile flow rate function for numerical models. The final section of the ventricular system after the fourth ventricle is selected for the flow output location. We set the normal baseline CSF pressure at 500 Pa and the pathological baseline at 2700 Pa [6].

1.4. Boundary Conditions

The deformable boundaries (walls) of the ventricular system are subjected to the fluid-solid interface constraints

$$d_i^f = d_i^s; \tag{1}$$

$$n\tau_{ij}^f = n\tau_{ij}^s; \tag{2}$$

$$u = \dot{d}_i^s. \tag{3}$$

Equalities (1), (2) display displacement and stress compatibility within the fluid-solid interface. Equation (3) signifies the equality between the CSF velocity u and solid wall velocity $\dot{d}_i^s$ on the interface [8]. On all interfaces, except for the fluid-solid interface, no-slip boundary conditions are applied. To ensure accurate solutions of the numerical simulations, we performed a study of mesh independence and computations on various meshes. Finally, we chose an unstructured mesh, with a range of 0.05 to 0.35 mm in edge lengths.

2. RESULTS

The results of numerical and experimental investigations of the CSF and brain tissue of NCH patients are presented below.

2.1. Comparison of Simulated and Experimental Data

The diagrams of the CSF velocity V in the AS acquired from CINE PC-MRI data for all cases are compared in Fig. 2 with the CSF numerical simulated velocity data (N is the part of the cardiac cycle). It is worth noting that the errors of matching the amplitude values and the frequency of the simulated CSF velocity diagrams with the CSF velocity diagrams acquired from CINE PC-MRI in all cases were smaller than 8.9 and 3.2%, respectively. These results show that the numerical simulation is confirmed by the in vivo CSF velocity measurements. In addition, more detailed CSF flow information can be predicted by the presented numerical simulation than the MRI measurement technique.

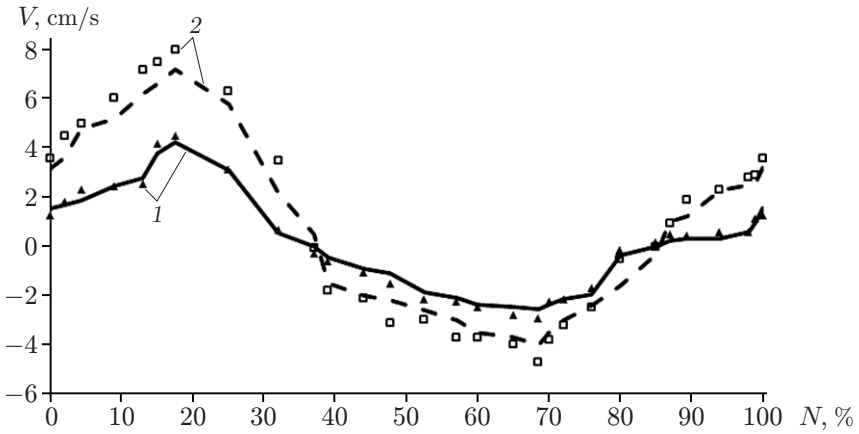

Fig. 2. CSF velocity distributions for the healthy subject (*1*) and patient No. 1 (*2*): the curves and points are the results of simulations and experiments, respectively.

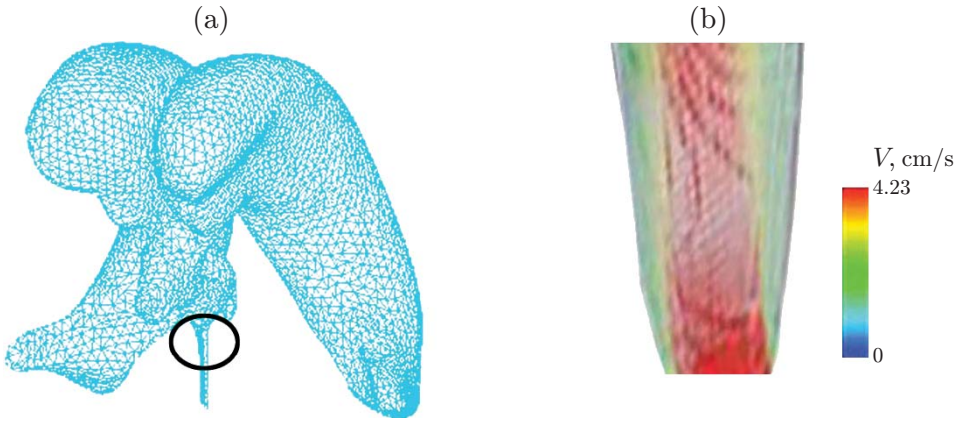

Fig. 3. CSF velocity distribution in the AS of the healthy subject for $N = 17.5\%$ based on numerical simulation results: (a) AS; (b) zoomed AS fragment.

2.2. Dimensional Analysis

The average areas of the patients' brains and ventricular systems were $S_b = (766.9 \pm 71.9)$ cm^2 and $S_v = (304.6 \pm 7.3)$ cm^2, respectively. The average volumes of the patients' brains and ventricular systems were $V_b = (1080.8 \pm 83.2)$ cm^3 and $V_v = (291.2 \pm 10.3)$ cm^3, respectively. The average volume of the ventricular systems of seven patients was 15.6 times larger than that in the healthy subject. In comparison, this parameter was 13.3 in [6] and 17.7 in [5]. The brain volume in the healthy subject was 1175.2 cm^3. Therefore, this value decreased due to the NCH by 8%, while the volume of the ventricles increased significantly. The greatest change was observed in the area of the walls of the ventricular system.

2.3. CSF Velocity and Reynolds Number

Figure 3 shows the mid-systole phase at $N = 17.5\%$ of the cardiac cycle, where the CSF has a relatively high velocity (4.23 cm/s for the healthy subject) in the AS. This value is consistent with that obtained by Ünal et al [10]. The CSF velocity in the AS during the diastole phase at 68% of the cardiac cycle is relatively low (see Fig. 2). The average CSF velocity in patients' AS was 51% of the mean CSF velocity in healthy subject's AS (see the table). The average velocity was calculated as the mean arithmetic value of the minimum and maximum CSF velocities in the AS for seven patients.

Mean pressures $\bar{p}_{AS}$ and $\bar{p}_{LV}$ and mean pressure amplitudes $\bar{A}_{AS}$ and $\bar{A}_{LV}$ in the AS and lateral ventricle, peak CSF velocity $V_{\max}$ in the AS, and Reynolds numbers Re in the AS before and after shunting based on numerical simulation results

Patient number	$\bar{A}_{AS}$, Pa	$\bar{p}_{AS}$, Pa	$\bar{A}_{LV}$, Pa	$\bar{p}_{LV}$, Pa	$V_{\max}$, cm/s	Re	
						Before shunting	After shunting
1	117.8	2722.7	120.4	2716.5	7.2	416.7	340.1
2	134.6	2647.2	128.5	2639.8	5.1	399.6	317.9
3	125.6	2764.8	122.9	2760.2	8.9	422.1	—
4	137.6	2882.3	142.5	2876.8	7.4	417.8	—
5	118.2	2911.3	119.8	2900.2	4.2	392.8	—
6	138.5	2696.3	135.7	2687.6	7.6	419.6	—
7	131.6	2885.1	141.6	2876.7	4.3	393.8	—

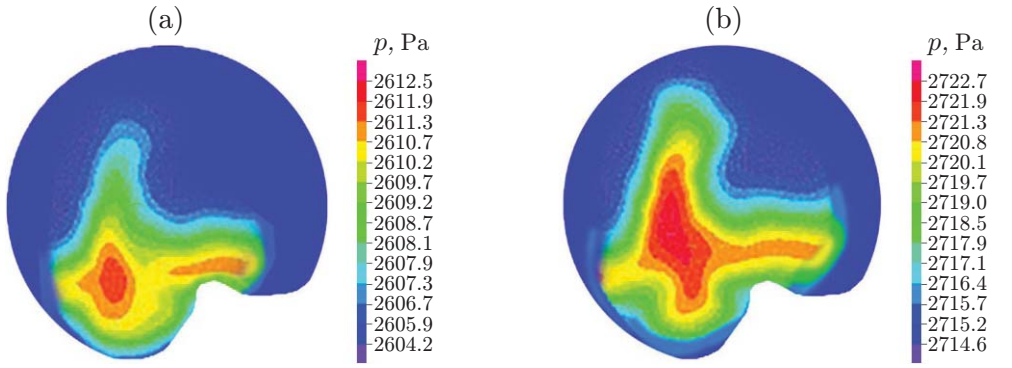

Fig. 4. CSF pressure distributions for patient No. 1 based on numerical simulations: (a) $N = 17.5\%$; (b) $N = 84\%$.

The maximum Reynolds number in the healthy subject was about 311. Siyahhan et al. [11] reported the value Re = 300. The average Reynolds number in the patients was 409 (see the table). Nevertheless, this value is within the range of the Reynolds numbers for the laminar flow.

2.4. CSF Pressure Distributions

The maximum CSF pressure of the healthy subject was 530.1 Pa at $N = 84\%$ and occurred in the AS. This is consistent with the results of previous studies [11].

The CSF pressure distribution of patient No. 1 is plotted in Fig. 4. The average CSF pressures in the AS and lateral ventricle of seven patients were (2787.1 ± 105.3) and (2779.7 ± 104.7) Pa, respectively (see the table). The average CSF pressure in the AS of the NCH patients was approximately 5.3 times greater than that in the healthy subject.

The measured CSF pressure amplitudes $p_{\max} - p_{\min}$ in the AS of the patients and that of the healthy subject were found to be (129.1 ± 8.7) and 66.2 Pa, respectively (see the table), i.e., the average CSF pressure amplitude in the NCH patients is approximately twice greater than that in the healthy subject.

3. DISCUSSION

The values of the CSF pressure and velocity are listed in the table. The coefficient of variation (standard deviation divided by the average value) is less than 7.5% for the mean CSF pressure and CSF pressure amplitude, while its value is greater than 28% for the CSF velocity, indicating the more limited range of pressure. Therefore, the pressure is a preferred index for comparisons of disease conditions before and after treatment by shunting.

To evaluate the changes in the CSF pressure during the treatment, the computational simulation was repeated in three stages during the treatment (at 14, 91, and 730 days after shunting) for patient Nos. 1 and 2. The mean pressures in the AS of patient Nos. 1 and 2 on days 14, 91, and 730 were approximately 33.9, 68.9, and 73.4% smaller than the pre-shunting values, respectively.

Although, according to the reports of the attending physician, the symptoms of NCH on days 14 and 91 after shunting had entirely disappeared, the patients reported consistent headaches during this time interval. This became evident on day 14 after shunting, when patients' ventricle volumes were not significantly reduced, staying at 2 times the volume of the healthy subject; we speculate that this is due to residual strain on the brain tissue, despite the removal of all other NCH symptoms. This caused the patient to suffer considerable pain, until day 91 after shunting, by the time brain tissue had sufficient time to relax. By this time, the patient's ventricle volume was 130.1% of the ventricle volume of the healthy subject, and the patients' headaches were reduced. On day 730 after shunting, the attending physician reconfirmed the absence of all NCH symptoms; this time, the patients reporting no pain. By this day, the ventricle volume was only 116% of that of the healthy subject. This reduction demonstrated a return of the NCH patient's brain to a new healthy status with new pressure and volume values different from those in the healthy subject. The average Reynolds number in the AS of the patients was 329, clearly not completely returning to its pre-shunting value; however, the CSF flow remained laminar. Also, on day 730 after shunting, the percentage of ventricle volume reduction was two times greater than the percentage of pressure reduction. This means that the pressure was stable despite a continuous decrease in the ventricle volume.

CONCLUSIONS

A new non-invasive technique of CSF pressure measurements for NCH patients is proposed. These results would be valuable for understanding the mechanism of the healing process of NCH patients and can be used in the future for developing methods of CSF pressure measurements for NCH patients and for studying physiological changes after shunting.

REFERENCES

1. I. K. Pople, "Hydrocephalus and Shunts: What the Neurologist Should Know," J. Neurology, Neurosurgery Psychiatry **73**, i17–i22 (2002).
2. J. Malm, B. Kristensen, M. Fagerlund, et al., "Cerebrospinal Fluid Shunt Dynamics in Patients with Idiopathic Adult Hydrocephalus Syndrome," J. Neurology, Neurosurgery Psychiatry **67**, 273–277 (2009).
3. P. K. Eide and A. Brean, "Cerebrospinal Fluid Pulse Pressure Amplitude During Lumbar Infusion in Idiopathic Normal Pressure Hydrocephalus Can Predict Response to Shunting," Cerebrospinal Fluid Res. **7** (5), (2010).
4. E. E. Jacobson, D. F. Fletcher, M. K. Morgan, and I. H. Johnston, "Computer Modelling of the Cerebrospinal Fluid Flow Dynamics of Aqueduct Stenosis," Med. Biol. Engng Comput. **37**, 59–63 (1999).
5. A. A. Linninger, M. Xenos, D. C. Zhu, et al., "Cerebrospinal Fluid Flow in the Normal and Hydrocephalic Human Brain," IEEE Trans. Biomed. Engng. **54**, 291–302 (2007).
6. B. Sweetman, M. Xenos, L. Zitella, and A. A. Linninger, "Three-Dimensional Computational Prediction of Cerebrospinal Fluid Flow in the Human Brain," Comput. Biol. Med. **41**, 67–75 (2011).
7. O. Algin, B. Hakyemez, and M. Parlak, "Phase-Contrast MRI and 3D-CISS Versus Contrast-Enhanced MR Cisternography on the Evaluation of Spontaneous Third Ventriculostomy Existence," J. Neuroradiol. **38**, 98–104 (2011).
8. S. Gholampour, N. Fatouraee, A. S. Seddighi, and S. Oraee Yazdani, "A Hydrodynamical Study to Propose a Numerical Index for Evaluating the CSF Conditions in Cerebral Ventricular System," Intern. Clinical Neurosci. J. **1** (1), 1–9 (2014).
9. K. J. Streitberger, E. Wiener, J. Hoffmann, et al., "In Vivo Viscoelastic Properties of the Brain in Normal Pressure Hydrocephalus," NMR Biomedicine **24** (4), 385–392 (2011).
10. Ö. Ünal, A. Kartum, S. Avcu, et al., "Cine Phase-Contrast MRI Evaluation of Normal Aqueductal Cerebrospinal Fluid Flow According to Sex and Age," Diagnost. Intervent. Radiology **15**, 227–237 (2009).
11. B. Siyahhan, V. Knobloch, D. de Ze'licourt, et al., "Flow Induced by Ependymal Cilia Dominates Near-Wall Cerebrospinal Fluid Dynamics in the Lateral Ventricles," J. Roy. Soc. Interface **11**, 20131189 (2014).